Classification and rovibrational normal modes of $3l3l'3l''$ triply excited states of atoms

Toru Morishita[1] and C. D. Lin[2]
[1]*Department of Applied Physics and Chemistry, University of Electro-Communications, 1-5-1, Chofu-ga-oka, Chofu-shi, Tokyo 182-8585, Japan*
[2]*Department of Physics, Cardwell Hall, Kansas State University, Manhattan, Kansas 66506*
(Received 6 February 2001; revised manuscript received 10 May 2001; published 5 October 2001)

We analyze the angular correlation of the 64 intrashell $3l3l'3l''$ states of a model atom with the three electrons confined on the surface of a sphere. Each wave function is examined in the body-fixed frame of the atom to search for the basic normal modes of the collective motion of the three electrons. Contour surfaces are used to display the interelectronic density distributions and nodal surfaces. It is shown that the calculated energy levels can be grouped into rotational patterns similar to those of a symmetric top. Three different basic normal modes of the joint motion of the three electrons are identified. For the higher states excitations of these three basic modes have also been discovered. Based on these normal modes we have classified all the 64 $3l3l'3l''$ states into manifolds of truncated rotational states of a symmetric top. The classification scheme is then used to group the $3l3l'3l''$ states of N^{4+} and the $1s^2 3l3l'3l''$ states of N^{2+} calculated by Vaeck and Hansen [J. Phys. B **25**, 883 (1992)], to show that their rotational level structures are similar to those of the model atom with very few modifications.

DOI: 10.1103/PhysRevA.64.052502 PACS number(s): 31.25.Jf, 31.10.+z, 31.15.Hz, 31.30.−i

I. INTRODUCTION

The properties of singly excited states of a many-electron atom are well understood. Within the shell model based on the independent particle picture, the wave function of the outermost electron is analogous to the familiar hydrogenic wave function. When two electrons are simultaneously excited, the independent particle picture fails. Over the last three decades a number of theoretical approaches have been developed to describe these doubly excited states [1–5]. The picture that has emerged is that the motion of the two electrons has to be treated jointly and the excitation spectrum of doubly excited states may be understood qualitatively in terms of the quanta of rotation and vibration of a floppy linear triatomic molecule. Furthermore, a set of different quantum numbers have been proposed [2] to classify these doubly excited states. Such classifications have now been widely used in the literature to replace the quantum numbers based on the independent electron model. The most important consequence of these quantum numbers is that they allow doubly excited states to be rearranged into new order and a number of propensity rules have also been elucidated [see Ref. [1] and references therein].

In the last few years, efforts have been made toward the understanding of triply excited states of atoms [6–12]. With synchrotron radiation light sources, triply excited states of the Li atom have been investigated in many experiments [13–16]. For collisions of multiply charged ions with multielectron targets, triply excited states are also populated through multiple electron capture processes. At the same time, a number of theoretical methods have been extended to obtain accurate energies and widths of selective triply excited states [17–21]. Most of these theoretical and experimental works concentrated on the low-lying $2l2l'nl''$ triply excited states.

According to the shell model, there are 64 intrashell $3l3l'3l''$ triply excited states. The number of states identified or calculated for any particular species in general is very limited. A small number of them have been identified in synchrotron radiation experiments [22,23] and some of them have been calculated for Li [22,23] and for positive ions [24]. The most recent extensive calculations for the $3l3l'3l''$ states are the 11 states of He^- obtained by Nicolaides and Piangos [25]. Using the configuration-interaction approach, Vaeck and Hansen [26] obtained all the 64 intrashell $3l3l'3l''$ triply excited states of N^{4+} and of N^{2+}. They tried to classify the states they calculated using the description of the earlier paper by Watanabe and Lin [6] with only limited success.

When compared to doubly excited states of a two-electron atom, the addition of one more electron introduces three more spatial degrees of freedom and one more spin degree of freedom to the total wave function. Even when the spins are averaged, the electronic density is still represented by a function of nine variables. To understand correlation, which is a property of the relative motion of the electrons, one can examine the wave function in the body-fixed frame of the atom by averaging out the overall rotational motion with respect to the space-fixed axes. If one further defines the hyperradius that measures the size of the atom, one is still left with five coordinates which describe the relative positions of the three electrons at a fixed hyperradius. For the two-electron atom, the corresponding representation of the relative motion is described by a function of two variables. Such a two-variable function can easily be displayed graphically and the correlated motion can be visualized. For three-electron atoms, any casual partial display of such a function of five variables in two dimensions is useless unless proper coordinates that reveal the characteristics of individual triply excited states are identified. In other words, to understand the correlated motion of the three electrons, one would have to identify the approximate normal modes or normal coordinates that describe the triply excited states.

In several recent papers [9–12] we have examined the correlation of a three-electron atom in hyperspherical coordinates. For doubly excited states we have shown that, by averaging over the coordinates of the innermost electron, the correlations of the two outer electrons are similar to the corresponding doubly excited states of a two-electron atom. For intrashell triply excited states, we have shown that an entirely different display of the three-electron wave functions is necessary. Since triply excited states lie well above all the singly and doubly excited states, the calculation of the wave functions of triply excited states for a real three-electron atom such as Li is very complicated. Thus only the $2l2l'2l''$ triply excited states have been examined so far. There are eight such intrashell $2l2l'2l''$ triply excited states and they have been classified into three groups (see Ref. [9]).

In this paper our goal is to study the correlation of the $3l3l'3l''$ triply excited states, with the aim of identifying the normal modes of the angular motion of the three electrons and assessing the possibility of classifying these states. With this in mind we need to find an efficient method to generate all 64 wave functions. Since we limit ourselves only to intrashell states, it is more convenient to study the wave functions of a model atom of three electrons on the surface of a sphere with the nucleus at the center [6,7,27–29]. In this model there are no intershell states and the intrashell states can be readily obtained. Furthermore, by freezing the radial degrees of freedom, each wave function is described by six angular variables only. By averaging out the overall rotation of the model atom with respect to the space-fixed frame, the correlated motion of the three electrons is represented by a function of three variables. We examine to what extent such motion can be approximated as the rotation and vibration of an XY_3 molecule. Since electrons are very light, the correlated motion can at most be close to that of a very floppy molecule. In other words, deviations from a rigid symmetric top description are expected to be large. Nevertheless, our goal is to ''extract'' the basic normal modes of the model atom and then classify the model atom eigenstates using these normal modes. We then explore to what extent the $3l3l'3l''$ triply excited states of a real atom can be similarly classified using the normal modes of the model atom.

This is not the first time that such a model has been used to analyze the correlation of intrashell triply excited states. In Ref. [6], a similar but simplified model was used where the independent electron motion was averaged out and only the interelectronic interactions were considered. Furthermore, the range of the angular momentum of each electron in constructing the basis functions was limited to $l \leqslant 2$ only. The calculated energy levels were analyzed using the D_{3h} symmetry group. Based on such a model, a small subset of the calculated energy levels were grouped into a rotational multiplet similar to that of a symmetric top. The states within each rotational multiplet were shown to exhibit common features by displaying the wave functions or densities in one of the coordinates of the model atom. In that early model, many of the higher $3l3l'3l''$ triply excited states were left as ''residues'' since the dominant features of these higher states were not easy to unravel. In a subsequent paper, Bao *et al.* [7] reexamined the intrashell states using the same model as the present one, but in constructing the basis functions the range of the angular momentum of each electron was limited to $l \leqslant 3$ only. In [7], the symmetry properties of the wave functions in the body-fixed frame were analyzed, following the earlier works of Bao and co-workers [27–29]. However, the classification of the states was not addressed. To make the classification possible, one would need to calculate all the $3l3l'3l''$ states accurately, and develop an efficient method of identifying the similarities of the states belonging to the same group. This is not trivial since the breakdown of symmetry for the excited states is quite large in general, and our goal is to identify features that would allow us to assign states into the same group, such that order will emerge.

In the present paper, we analyze the wave functions of the model atom for states of arbitrary L, S, and π, the total orbital and spin angular momentum quantum numbers and the parity, respectively. As stated earlier, by confining each electron to the surface of a sphere of radius r_0, there are only six spatial degrees of freedom in the model atom. By expanding the wave function in the body-fixed frame to remove the overall rotation, the relative motion of the three electrons is then governed by a function of three variables. By defining the quantization axis of the body-fixed frame to be perpendicular to the plane formed by the three electrons, the absolute value of the projection of L along this body-fixed frame axis, to be called T, will be a good quantum number if the model atom can be approximated as a rigid body. We then examine the density distributions of the electrons from the calculated wave functions to reveal states that have similar distributions, as represented by their approximate normal modes and/or nodal surfaces, and then arrange the energy levels of states in the same group into rotational multiplets, with each multiplet resembling the rotational levels of a symmetric top. In the process we will show that quantum symmetry, i.e., the symmetry imposed by the Fermi statistics, and the symmetries represented by the good quantum numbers L, S, and π, play a major role in determining the approximate normal modes of these states [6,7]. A brief account of the normal modes for such a model atom has been presented elsewhere [30]. With these normal modes identified we show that the energy levels of the model atom can be classified. We then show that the energy levels of the $3l3l'3l''$ intrashell triply excited states of N^{4+} and of N^{2+} calculated by Vaeck and Hansen [26] can be similarly classified with little modifications.

The rest of this paper is arranged as follows. In Sec. II we first describe the model atom and the calculation and analysis of wave functions in the body-fixed frame. We then define the angles to be used for the visualization of angular correlations of the body-fixed frame wave functions. In Sec. III we present the analysis and the resulting classifications of the model atom. In Sec. IV the classification scheme is then used to classify the $3l3l'3l''$ intrashell triply excited states of N^{4+} and of N^{2+}. A short summary is given in Sec. V.

II. THE MODEL ATOM—THREE ELECTRONS ON THE SURFACE OF A SPHERE

A. The model Hamiltonian and the calculations of eigenstates

In this model, we freeze the radial degrees of freedom of the three electrons. The Hamiltonian of the model atom in atomic units then reads

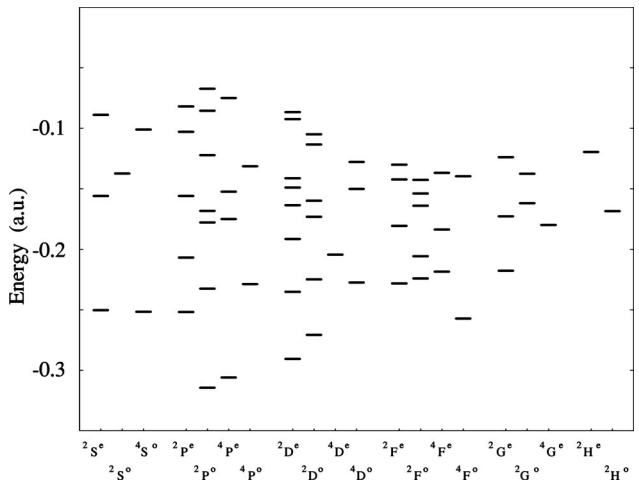

FIG. 1. Energy levels of the 64 $3l3l'3l''$ triply excited states of a model atom ordered along each column according to the $^{2S+1}L^{\pi}$ symmetry. The relative order of the spectra exhibits no regularity. The numerical eigenvalue of each state is given in Table I.

$$H=\frac{1}{2r_0^2}\sum_{i=1}^{3}\hat{\ell}_i^2+\frac{1}{r_0}\sum_{i>j}\frac{1}{|\hat{\mathbf{r}}_i-\hat{\mathbf{r}}_j|}-\frac{3Z}{r_0}, \tag{1}$$

where Z is the effective nuclear charge, $\hat{\ell}_i$ is the angular momentum operator of the ith electron with respect to the nucleus, $\hat{\mathbf{r}}_i$ is the unit vector pointing from the nucleus to the ith electron, and r_0 is the radius of the sphere. We use $Z=1.423$ and $r_0=6.326$ a.u. to simulate the $N=3$ shell of the intrashell states of He^- [6,7]. The calculated energy eigenvalues depend on the choice of r_0. However, the relative order is not expected to change with r_0. We note that the electron-nucleus interaction term $-3Z/r_0$ only adds an overall constant and does not affect the relative order of the eigenenergies.

The eigenstates of the Hamiltonian (1) are labeled by the good quantum numbers L, S, and π. The total wave function ψ is antisymmetric under exchange of any two electrons and can be written as

$$\psi=\sum_{S_{12}}\Phi_{LM}^{S,S_{12}}(\hat{\mathbf{r}}_1,\hat{\mathbf{r}}_2,\hat{\mathbf{r}}_3)\chi_{S_{12}}^{S}, \tag{2}$$

where $\chi_{S_{12}}^{S}=[\{\chi(1)\chi(2)\}^{S_{12}}\chi(3)]^{S}$ is the coupled spin function of the three electrons with intermediate spin S_{12}. The spatial function $\Phi_{LM}^{S,S_{12}}(\hat{\mathbf{r}}_1,\hat{\mathbf{r}}_2,\hat{\mathbf{r}}_3)$ is obtained by diagonalizing in a basis of $[\{Y_{l_1}(\hat{\mathbf{r}}_1)Y_{l_2}(\hat{\mathbf{r}}_2)\}^{l_{12}}Y_{l_3}(\hat{\mathbf{r}}_3)]^{LM}$, which is the coupled orbital angular momentum of the three electrons with intermediate angular momentum l_{12}. To obtain accurate energies of the $3l3l'3l''$ states the maximum value of each l has been set to 7 in the calculation.

The selected 64 eigenenergies thus obtained for the model He^- ($N=3$) are displayed on a level diagram in Fig. 1, ordered along each column in increasing energies for each set of L, S, and π. The numerical energy eigenvalues are given in Table I. Clearly the ordering of energy levels appears to be rather erratic. It is our goal to rearrange these levels such that the regularity of the levels will emerge. At this point, we emphasize that configuration mixing for these states is quite large and the shell model designation is completely inadequate and meaningless. One of the methods of finding a classification scheme is to identify states that have common features. In particular, one would like to group states that have nearly identical internal structure, or correlations, among the three electrons. To do this we need to find a way to visualize them.

B. Body-frame wave functions and internal angles

The wave functions obtained from the calculations above are expressed in a laboratory-fixed frame. Since we are interested in the relative positions of the three electrons and the nucleus of the model atom, the overall rotation of the three electrons with respect to the fixed laboratory frame is not important. To examine correlations one could average over the rotational motion of the whole atom or examine the wave functions in the body-fixed frame. Thus we analyze the wave function in the body-fixed frame following Watanabe and Lin [6] and Bao *et al.* [7]. Define the body-fixed frame axes by

$$\mathbf{S}_z=\mathbf{r}_1\times\mathbf{r}_2+\mathbf{r}_2\times\mathbf{r}_3+\mathbf{r}_3\times\mathbf{r}_1,$$

$$\mathbf{S}_y=\frac{\sqrt{3}}{2}(\mathbf{r}_1-\mathbf{r}_2), \tag{3}$$

$$\mathbf{S}_x=\mathbf{S}_y\times\mathbf{S}_z.$$

The body-fixed frame z axis thus defined is perpendicular to the plane formed by the three electrons and we choose this axis to go through the nucleus as well.

Each spatial wave function $\Phi_{LM}^{S,S_{12}}(\hat{\mathbf{r}}_1,\hat{\mathbf{r}}_2,\hat{\mathbf{r}}_3)$ [Eq. (2)] in the space-fixed frame can be expanded in terms of body-fixed frame component wave functions $\varphi_{LQ}^{S,S_{12}}(\Omega_I)$ through a general rotation

$$\Phi_{LM}^{S,S_{12}}(\hat{\mathbf{r}}_1,\hat{\mathbf{r}}_2,\hat{\mathbf{r}}_3)=\sum_{Q=-L}^{L}\varphi_{LQ}^{S,S_{12}}(\Omega_I)D_{QM}^{(L)}(\omega), \tag{4}$$

where $D_{QM}^{(L)}(\omega)$ is the rotation matrix for the frame transformation, and Q and M are the azimuthal components of L in the body-fixed frame and in the space-fixed frame, respectively. Here ω represents the three Euler angles defining the orientation of the body-fixed frame axes with respect to the laboratory-fixed frame axes and Ω_I is a set of three internal angles to represent the "shape" of the system, to be specified below.

From the symmetry property of the rotation matrix $D_{QM}^{(L)}(\omega)$, the body-fixed frame wave function satisfies the following relation [6]:

TABLE I. Energy levels, present classifications, and fractions of the rotational decomposition A_T of the 64 states calculated for the model atom to represent the $3l3l'3l''$ intrashell triply excited state of He^-.

States	Group-T	Energy (a.u.)	A_T					
			$T=0$	$T=1$	$T=2$	$T=3$	$T=4$	$T=5$
$^2S^e$		$(3s3p^2,3s3d^2,3p^23d)$						
(1)	C-0	−0.250	1.000					
(2)	Cc-0	−0.156	1.000					
(3)	Ccc-0	−0.089	1.000					
$^2S^o$		$(3p3d^2)$						
(1)	CB-0	−0.137	1.000					
$^4S^o$		$(3p^3,3p3d^2)$						
(1)	B-0	−0.252	1.000					
(2)	Bb-0	−0.101	1.000					
$^2P^e$		$(3s3p^2,3s3d^2,3p^23d,3p^23d,3d^3)$						
(1)	B-1	−0.252	0.313	0.687				
(2)	C-0	−0.207	0.673	0.327				
(3)	CB-1	−0.156	0.482	0.518				
(4)	Bb-1	−0.103	0.213	0.787				
(5)	Cc-0	−0.082	0.562	0.438				
$^2P^o$		$(3s^23p,3s3p3d,3s3p3d,3p3d^2,3p3d^2,3p^3,3p^23d)$						
(1)	A-1	−0.314	0.000	1.000				
(2)	C-1	−0.233	0.022	0.978				
(3)	Ab-1	−0.178	0.126	0.874				
(4)	Ac-1	−0.168	0.320	0.680				
(5)	Cc-1	−0.122	0.074	0.926				
(6)	Acc-1	−0.085	0.357	0.643				
(7)	Ccc-1	−0.067	0.040	0.960				
$^4P^e$		$(3s3p^2,3s3d^2,3p^23d,3d^3)$						
(1)	A-0	−0.306	1.000	0.000				
(2)	Ab-0	−0.175	0.702	0.298				
(3)	Ac-0	−0.152	0.715	0.285				
(4)	CB-1	−0.075	0.419	0.581				
$^4P^o$		$(3s3p3d,3p3d^2)$						
(1)	C-1	−0.229	0.000	1.000				
(2)	Cc-1	−0.131	0.000	1.000				
$^2D^e$		$(3s^23d,3s3p^2,3s3d^2,3p^23d,3p^23d,3p^23d,3p^23d,3d^3)$						
(1)	A-2	−0.291	0.020	0.003	0.977			
(2)	B-1	−0.235	0.074	0.518	0.408			
(3)	C-2	−0.192	0.370	0.170	0.460			
(4)	C-0	−0.163	0.250	0.289	0.461			
(5)	Ab-2	−0.149	0.253	0.267	0.480			
(6)	Ac-2	−0.141	0.075	0.165	0.760			
(7)	Cc-2	−0.092	0.135	0.246	0.619			
(8)	Bb-1	−0.087	0.244	0.500	0.256			

TABLE I. (*Continued*).

States	Group-T	Energy (a.u.)	A_T					
			$T=0$	$T=1$	$T=2$	$T=3$	$T=4$	$T=5$
$^2D^o$		$(3s3p3d,3s3p3d,3p3d^2,3p3d^2,3p3d^2,3p^3)$						
(1)	A-1	−0.271	0.000	0.991	0.009			
(2)	B-2	−0.225	0.000	0.223	0.777			
(3)	Ab-1	−0.173	0.289	0.539	0.172			
(4)	C-1	−0.160	0.015	0.783	0.202			
(5)	Ac-1	−0.113	0.183	0.778	0.039			
(6)	Cc-1	−0.105	0.073	0.490	0.437			
$^4D^e$		$(3p^23d)$						
(1)	C-2	−0.204	0.000	0.029	0.971			
$^4D^o$		$(3s3p3d,3p3d^2,3p3d^2)$						
(1)	B-0	−0.227	0.613	0.387	0.000			
(2)	C-1	−0.150	0.285	0.693	0.021			
(3)	CB-2	−0.128	0.030	0.289	0.681			
$^2F^e$		$(3s3d^2,3p^23d,3p^23d,3d^3)$						
(1)	A-2	−0.228	0.063	0.014	0.921	0.002		
(2)	B-1	−0.181	0.056	0.588	0.348	0.009		
(3)	C-0	−0.142	0.285	0.158	0.359	0.198		
(4)	C-2	−0.130	0.024	0.117	0.574	0.285		
$^2F^o$		$(3s3p3d,3p3d^2,3p3d^2,3p3d^2,3s3p3d)$						
(1)	A-1	−0.223	0.002	0.800	0.016	0.182		
(2)	B-2	−0.200	0.025	0.034	0.424	0.517		
(3)	C-3	−0.164	0.007	0.216	0.015	0.763		
(4)	C-1	−0.143	0.072	0.419	0.299	0.211		
(5)	Ab-1	−0.142	0.005	0.328	0.318	0.348		
$^4F^e$		$(3s3d^2,3p^23d,3d^3)$						
(1)	A-0	−0.219	0.684	0.003	0.223	0.090		
(2)	B-3	−0.184	0.185	0.017	0.040	0.759		
(3)	Ab-0	−0.137	0.449	0.422	0.127	0.002		
$^4F^o$		$(3s3p3d,3p3d^2)$						
(1)	A-3	−0.257	0.000	0.021	0.000	0.979		
(2)	C-1	−0.140	0.000	0.542	0.255	0.203		
$^2G^e$		$(3s3d^2,3p^23d,3d^3)$						
(1)	A-4	−0.218	0.003	0.006	0.035	0.001	0.955	
(2)	A-2	−0.173	0.079	0.017	0.589	0.013	0.303	
(3)	B-1	−0.123	0.053	0.479	0.184	0.100	0.185	
$^2G^o$		$(3p3d^2,3p3d^2)$						
(1)	A-1	−0.162	0.000	0.588	0.036	0.209	0.167	
(2)	B-4	−0.138	0.004	0.230	0.029	0.036	0.702	
$^4G^o$		$(3p3d^2)$						
(1)	A-3	−0.180	0.030	0.100	0.003	0.866	0.001	
$^2H^e$		$(3d^3)$						
(1)	A-4	−0.120	0.015	0.028	0.100	0.002	0.845	0.009
$^2H^o$		$(3p3d^2)$						
(1)	A-5	−0.168	0.001	0.005	0.007	0.038	0.003	0.946

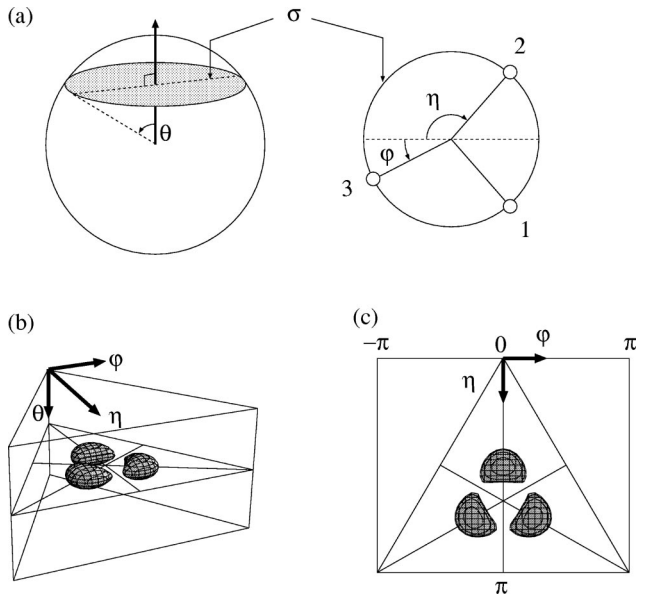

FIG. 2. (a) Definition of the three angles used to describe the relative positions of the three electrons on a sphere. (a) The three electrons form a σ plane. The position of this plane with respect to the nucleus is measured by θ. On the plane, two angles as defined in the figure specify the shape of the triangle formed by the three electrons. The probability distribution of the three electrons on the surface is represented by the density distribution of the three angles (θ,η,ϕ). (b) Contour surfaces are used to represent the density distributions. (c) Top view of the contour surface to indicate the range of the two angles η and ϕ.

$$\varphi^{S,S_{12}}_{L-Q}(\Omega_I)=\pi(-1)^{L+Q}[\varphi^{S,S_{12}}_{LQ}(\Omega_I)]^*, \tag{5}$$

where $\pi=\pm 1$ is the parity of the system. Thus it is convenient to define $T=|Q|$ and analyze the T component $(0\leqslant T\leqslant L)$ of the body-fixed frame wave functions only.

To elucidate electron correlations for a three-electron system, the three internal angles Ω_I should be chosen as democratically as possible. We follow the choice of these three angles used in Refs. [7,11,12]. Referring to Fig. 2, define the plane of the three electrons as the σ plane. The body-fixed frame z axis is perpendicular to this plane and passing through the nucleus as in Eq. (3). On the σ plane, the three electrons are confined to a circle (see Fig. 2). We need two more angles to specify the shape of the triangle formed by the three electrons. From Fig. 2(a), define η to be half of the angle between electrons 1 and 2, measured along the arc where electron 3 lies. The angle ϕ measures the position of electron 3 from the line bisecting electrons 1 and 2 (the y axis in the body-fixed frame). When $\phi=0$, the three electrons form an isosceles triangle. If $\eta=2\pi/3$ and $\phi=0$, then the three electrons form an equilateral triangle. When $\theta=\pi/2$, the nucleus lies on the plane of the three electrons and these electrons are called coplanar. From these definitions, the ranges of the angles are $(0\leqslant\theta\leqslant\pi,\ 0\leqslant\eta\leqslant\pi,\ -\eta\leqslant\phi\leqslant\eta)$ [see Fig. 2(c)]. These three angles specify a definite shape of the triangle and the position of the triangle with respect to the nucleus. In other words, these three angles uniquely specify the relative positions of the three electrons and the nucleus. We note that, for a small ϕ, $\eta\sim\pi/2$ implies a triangle with a large base, and $\eta\sim\pi$ implies a triangle with a small base.

From Eqs. (2) and (4) one can define a density distribution function for each rotational component,

$$\rho_T(\Omega_I)=\begin{cases}\displaystyle\sum_{S_{12}}|\varphi^{S,S_{12}}_{LQ}(\Omega_I)|^2 & (T=0),\\ \displaystyle\sum_{S_{12}}[|\varphi^{S,S_{12}}_{L-Q}(\Omega_I)|^2+|\varphi^{S,S_{12}}_{LQ}(\Omega_I)|^2] & (T\neq 0).\end{cases} \tag{6}$$

This function depends only on the internal angles Ω_I and the sum over all the rotational components $0\leqslant T\leqslant L$ gives the total internal density distribution. This function specifies the shape of the three-electron atom. The summation is over the intermediate coupled spin S_{12}, i.e., $S_{12}=1$ for quartet states, and $S_{12}=0$ and 1 for doublet states. When the density for each individual intermediate spin component is specified, we call the part associated with $S_{12}=1$ the triplet parent component, and the part associated with $S_{12}=0$ the singlet parent component.

To give a numerical measure of the composition of the rotational components we define

$$A_T=\int\rho_T(\Omega_I)d\Omega_I, \tag{7}$$

where the integration is over the three internal angles $\Omega_I=(\theta,\eta,\phi)$ defined earlier. [Actual integrations were carried out using another set of internal coordinates $(\cos\theta_{12}=\mathbf{r}_1\cdot\mathbf{r}_2,\ \cos\theta_{13}=\mathbf{r}_1\cdot\mathbf{r}_3,\ \phi_{23}=\phi_3-\phi_2)$.] Clearly the sum of A_T over all possible values of T is unity. For convenience we will call A_T the rotational fraction. We say that A_T measures the purity of the rotational decomposition of the body-fixed frame wave function. When A_T is close to 1, T is considered to be an approximate good quantum number and can be used to label the state. We emphasize that A_T depends on the choice of the body-fixed frame quantization axis and there is no *a priori* reason to expect that T is an approximate good quantum number. On the other hand, if the three electrons act together like a rigid body, the atom will look like a rigid symmetrical top and T, being the projection along one of the principal axes, will be a good quantum number. For the three electrons, the density distribution is expected to be very floppy in view of the lightness of the electrons. The density distribution itself gives further information about the normal modes of the internal motion. We examine whether the rotational density distribution $\rho_T(\Omega_I)$ reveals such modes. For this purpose we need to be able to visualize $\rho_T(\Omega_I)$.

The density distribution $\rho_T(\Omega_I)$ is a function of three internal angles $\Omega_I=(\theta,\eta,\phi)$. Such a function of three variables is not easily displayed. We choose to display the contour surfaces. Figure 2(b) shows such a surface. A contour surface can display the dominant features of a function of three variables only if the function itself is relatively simple and monotonic. In Fig. 2(b) the plot is for a surface where the functional value is 60% of the maximum. The surface

TABLE II. Nodal surfaces in the real part (Re) and the imaginary part (Im) of the rotational components of spin specified wave functions $\varphi_{LQ}^{S,S_{12}=1}$ in the body-fixed frame resulting from the inherent quantum symmetry as analyzed by Bao *et al.* [7]. A black box denotes a forbidden component which is prohibited by symmetry. A blank box denotes a nodeless component which has no nodal surfaces due to the inherent symmetry. The symbol s implies that there is a nodal surface when the three electrons form an isosceles triangle with the two spin-parallel electrons at the base. The symbol S is used to indicate that a nodal surface appears whenever the three electrons form an isosceles triangle, irrespective of which two are at the base. The symbol d implies that there is a nodal surface when the plane of the three electrons coincides with the nucleus. The symbol h implies that, while the isosceles triangle is allowed, an inherent nodal surface appears when the three electrons form an equilateral triangle. s and S denote the swing modes, while d and h denote the d-type oscillation and the hinge mode, respectively. Adapted from Table I of Bao *et al.* [7].

	$\mathrm{Re}(\varphi_{L0})$	$\mathrm{Im}(\varphi_{L0})$	$\mathrm{Re}(\varphi_{L1})$	$\mathrm{Im}(\varphi_{L1})$	$\mathrm{Re}(\varphi_{L2})$	$\mathrm{Im}(\varphi_{L2})$	$\mathrm{Re}(\varphi_{L3})$	$\mathrm{Im}(\varphi_{L3})$	$\mathrm{Re}(\varphi_{L4})$	$\mathrm{Im}(\varphi_{L4})$	$\mathrm{Re}(\varphi_{L5})$	$\mathrm{Im}(\varphi_{L5})$
$^2S^e$	s											
$^2S^o$		d+h										
$^2P^e$		h	d+s	d								
$^2P^o$	d+s		s									
$^2D^e$	s		d+s	d	s							
$^2D^o$		d+h	s		d+s	d						
$^2F^e$		h	d+s	d	s		d+s	d+h				
$^2F^o$	d+s		s		d+s	d	s	h				
$^2G^e$	s		d+s	d	s		d+s	d+h	s			
$^2G^o$		d+h	s		d+s	d	s	h	d+s	d		
$^2H^e$		h	d+s	d	s		d+s	d+h	s		d+s	d
$^2H^o$	d+s		s		d+s	d	s	h	d+s	d	s	
$^4S^e$	S											
$^4S^o$		d										
$^4P^e$			d+s	d+h								
$^4P^o$	d+S		s	h								
$^4D^e$	S		d+s	d+h	s	h						
$^4D^o$		d	s	h	d+s	d+h						
$^4F^e$			d+s	d+h	s	h	d+s	d				
$^4F^o$	d+S		s	h	d+s	d+h	s					
$^4G^e$	S		d+s	d+h	s	h	d+s	d	s	h		
$^4G^o$		d	s	h	d+s	d+h	s		d+s	d+ h		
$^4H^e$			d+s	d+h	s	h	d+s	d	s	h	d +s	d+h
$^4H^o$	d+S		s	h	d+s	d+h	s		d+s	d+ h	s	h

would be a larger one if, say, the surface of 20% or 30% of the maximum was plotted. A contour surface of higher density would fit inside the surface.

From such density plots, the relative positions of the three electrons as well as the nucleus are partially displayed. For example, Fig. 2(b) shows that the maximum appears at $\theta = \pi/2$; thus the preferred positions of the three electrons are coplanar with the nucleus. The maximum also occurs along one of the diagonals. Thus the preferred shape of the three electrons is an isosceles triangle on the equatorial plane. In this example, the density distribution vanishes at ($\eta = 2\pi/3$, $\phi = 0$), meaning that the equilateral triangle is not allowed. The distribution can be viewed classically as a small oscillation of the third electron (in changing ϕ) or a hinge motion of the two other electrons (in changing η) [7,11]. The display of the density distributions and the existence of nodal surfaces allows us to assess the normal modes of the internal motion of the model atom. We will use such surface plots to examine the angular correlation pattern of the three electrons for all the $3l3l'3l''$ states calculated within the model.

C. Nodal surfaces of the body-fixed frame wave functions

Before proceeding to the classification of the calculated intrashell $3l3l'3l''$ states, it is advantageous to discuss what to expect. Recall that each state has a well-defined L, S, and π, and that the wave function is antisymmetric upon interchange of any pair of electrons. These symmetry conditions impose boundary conditions on the multidimensional wave function for each state and such conditions are reflected most clearly in the body-fixed frame wave functions. As an example, consider the coplanar geometry where the plane of the three electrons contains the nucleus. A rotation of π about the S_z axis is the same as the inversion of all three electrons. Therefore in this geometry the condition $(-1)^Q = \pi$ should be satisfied. In other words, if this condition is not satisfied, i.e., if $\pi(-1)^Q = -1$, the T component ($T = |Q|$) wave function should vanish at the coplanar geometry and thus $\theta = \pi/2$ is a nodal surface. Additional symmetry constraints can be obtained by considering the case of the three electrons forming an isosceles triangle or forming an equilateral triangle. Such constraints have been enumerated explicitly by Watanabe and Lin [6]. Bao *et al.* [7] further

considered the rotational components of two spin-up electrons and one spin-down electron, namely, triplet parent components with $M_S=1/2$. The results, summarized in Table I of Bao *et al.* [7], are reproduced here as Table II. This table will be used to assist the classification of the $3l3l'3l''$ states. Note that we analyze the nodal structure of the spin averaged densities $\rho_T(\Omega_I)$, but the analysis and the conclusions about the nodal surfaces of the rotational component wave functions are identical, since the singlet parent and triplet parent components for doublet states are related to each other according to the S_3 permutation group.

Table II shows that the spin-specified rotational component wave functions exhibit different kinds of nodal surface. The nodal surface at $\theta=\pi/2$ described in the previous paragraph is designated as d, implying an oscillation of the plane of the three electrons [the σ plane of Fig. 2(a)] with respect to the nucleus. An s implies that there is a nodal surface when the three electrons form an isosceles triangle with the two spin-up electrons at the base, i.e., $\phi=0$ is a nodal surface. From the mechanical viewpoint, an s is used to denote a swing mode. In this case the two spin-up electrons are fixed, with the spin-down electron swinging back and forth such that when the three electrons form an isosceles triangle the wave function vanishes. An h implies that there is a nodal surface orthogonal to the $\phi=0$ plane at $\eta=2\pi/3$. This mode is viewed as having the the spin-down electron fixed and the two spin-up electrons performing the motion of a hinge, moving toward or away from each other. In the density distribution $\rho_T(\Omega_I)$ defined in Eq. (6), the intermediate spin components are averaged out. Therefore it is not possible to separate s and h modes. These modes would result in a nodal surface when the three electrons form an equilateral triangle at ($\eta=2\pi/3$, $\phi=0$) [see Fig. 2(b)].

In Table II, a black box denotes a forbidden component that is prohibited by symmetry. A blank box denotes that there are no nodal surfaces imposed as the result of the symmetry constraints. Note that there are very few blank boxes, indicating that quantum symmetry indeed imposes severe constraints on the multielectron wave functions. In Table II we also notice components with two nodal surfaces, designated as d+s and d+h. These components have two nodal surfaces. For quartet states, S was used to denote a nodal surface when the three electrons form an isosceles triangle, irrespective of which two are at the base. The existence of three nodal surfaces implies higher energy. For the $3l3l'3l''$ states considered here there are no examples of S-type constraints.

D. Hierarchy of excitation energies and the "filling" of the rotational component wave functions

The total energy of the internal motion is decomposed into the potential energy and the kinetic energy of the internal degrees of freedom. Since a nodal surface implies higher kinetic energy, the low-lying states will "fill" rotational components which have the least number of nodal surfaces. Thus one can expect that low-lying states occur in those symmetries that have blank boxes in Table II and these states will "occupy" mostly the nodeless rotational components. For example, the $T=1$ component of $^2P^o$ has one blank box. From Table I, we note that the lowest $^2P^o$ state is almost 100% $T=1$, with a negligible $T=0$ component. The latter has two nodal surfaces of the d+s type, such that any $T=0$ component would contribute a higher energy to the state. Similarly, the $T=2$ component of $^2D^e$ has a blank box and this would be the preferred component for the lowest $^2D^e$ state. Indeed, from Table I we note that the lowest $^2D^e$ state has 97.7% of the $T=2$ composition. The lowest state "avoids" $T=0$ and $T=1$ because of the presence of nodal surfaces in these components.

III. ANALYSIS OF INTERNAL MODES OF THE 64 INTRASHELL $3l3l'3l''$ STATES

A. Energy levels

According to the shell model, there are 64 $3l3l'3l''$ triply excited electronic states in a three-electron atom. These states are labeled by the good quantum numbers L, S, and π. The configurations allowed by the Pauli exclusion principle for each symmetry are listed in Table I. They do not represent the eigenstates of the triply excited states since configuration interaction (CI) is expected to be very large. For the Hamiltonian Eq. (1) there exists an infinite number of eigenstates. In the present model calculation, for each L, S, and π, we "identify" $3l3l'3l''$ intrashell states to be the lowest eigenstates, where the number of states is given by the number of allowed intrashell states according to the shell model.

In Table I we list the properties of these 64 states calculated for the present model atom. For each symmetry, we first list all the configurations that can be coupled to the given L, S, and π according to the shell model. For example, there are five possible configurations for $^2P^e$ states, $3s3p^2$, $3s3d^2$, $3p^2(^3P^e)3d$, $3p^2(^1D^e)3d$, and $3d^3$. The energies of the first five states from the model calculation are ordered and the eigenenergies are listed in the third column. In the second column the present classification for each state is given. The classification is the final result of the present analysis, to be given below. The remaining columns give the rotational fraction A_T, as explained in Sec. II B [see Eq. (7)].

B. Group A

The first group of states are those that "occupy" predominantly the blank boxes in Table II. We designate these states to form group A. This group was denoted as A_1' in Ref. [6]. We will use a different designation here since the original designation does not provide a convenient way to denote higher excited states.

From Table II, by ordering the energies of the lowest states according to the T's where the blank occurs, we arrive at the rotational multiplet structure shown in the lower half of Fig. 3 where the ordering resembles the pattern of the rotational levels of a symmetric top. In the upper half of this figure, the contour surface of the density distribution $\rho_T(\Omega_I)$ of the corresponding T for each state is illustrated. Note that each figure is a simplified display of Fig. 2(b) in that only the equator plane has been drawn.

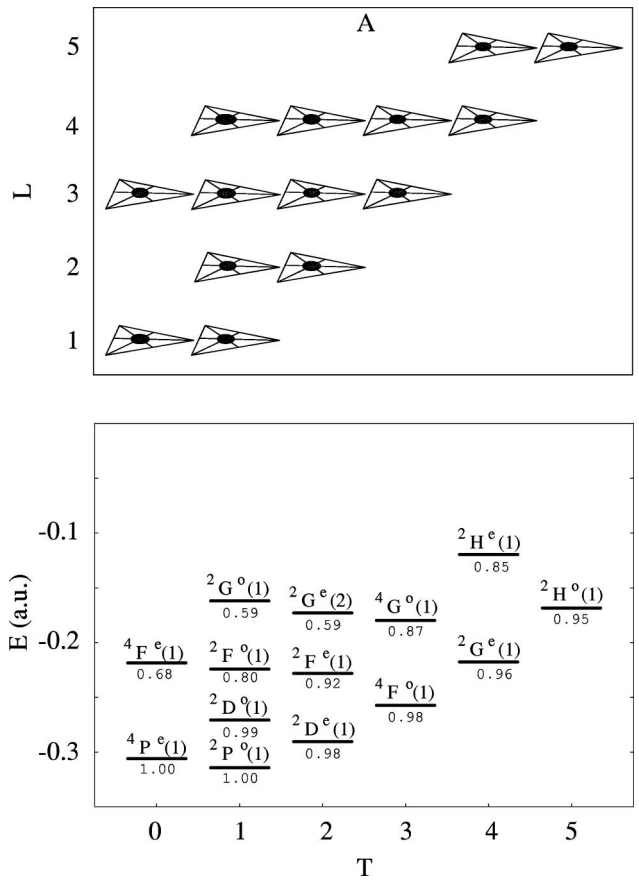

FIG. 3. Rotational levels and contour surface plots of the electronic density distribution for the $3l3l'3l''$ triply excited states that form group A. In the lower panel each state is denoted by its L, S, and π and the number n in parentheses indicates the nth state of that symmetry, with 1 being the lowest. The number below each level indicates the rotational fraction A_T [see Eq. (7)]. The contour surface plots in the upper frame give the density of the corresponding T components of the states in the lower frame. Each surface represents the equidensity surface of 60% of the maximum.

In the lower frame, each state is designated by its L, S, and π, plus a number n in parentheses indicating that it is the nth eigenstate of that symmetry. For group A, each state is the lowest one of the given symmetry except for $^2G^e$ where two states are in this group. The purity of the rotational decomposition A_T of each state is also indicated. Clearly the purity of each of the lower members is quite good. The minor rotational components are not forbidden, but are unfavorable because of the existence of nodal surfaces as imposed by symmetry. The purity deteriorates as L is increased. The deterioration is due to the centrifugal distortion of the electronic density distribution which resembles a floppy symmetric top.

The fact that the arrangement of energy levels shown in Fig. 3 resembles that of a symmetric top implies that the states have nearly identical effective moment of inertia, or, most likely, similar shape. To show that this is indeed the case, the contour surfaces of the density distributions for the states in this group are shown in the upper panel. These surfaces were drawn as described in Sec. II B. To emphasize the similarity, only the density of the dominant T component [that is, $\rho_T(\Omega_I)$] of each state is displayed. Each figure exhibits a maximum at the center ($\theta=\pi/2$, $\eta=2\pi/3$, $\phi=0$), meaning that the most preferred geometry is a coplanar equilateral triangle. Each surface is a plot of 60% of the maximum density. The size of the surface measures the floppiness of the coplanar equilateral triangle—the larger the surface, the more floppy the atom. Despite the mixture from other T components, it is interesting to note that the dominant T component for all the states in this group remains nearly the same. Thus we can say that in this group the three electrons form a coplanar equilateral triangle with the nucleus at the center. We note that the coplanar equilateral triangle is preferred by the model atom since the potential energy is minimum at this geometry. However, this geometry is not available to all the states, but only to those states shown in Fig. 3. We comment that states in group A have shape similar to that of a BF_3 molecule which is a coplanar equilateral triangle. However, for the BF_3 molecule, the zero-point oscillation around the equilibrium position is much smaller.

The density distribution of each of the states in group A looks like that of an oblate symmetric top. For an oblate symmetric top, the rotational energy is given by

$$E(L,T)=\frac{1}{2I}[2L(L+1)-T^2], \tag{8}$$

where I is the moment of inertia. Inspection of this formula shows that, for each fixed L, higher T has lower energy. This is confirmed in the calculated energies, as shown in Fig. 3. For each fixed T, this formula says that a state with higher L will have higher energy, which is also reflected in the calculated energies. On the other hand, a rigid symmetric top would predict that the energy difference between two successive L's is independent of T. The calculated energy levels do not obey this rule. This deviation reflects the fact that the three electrons do not form a rigid symmetric top, but rather a floppy one. The deviation is partially measured by T being not a good quantum number, which in turn is measured by the deviation of A_T away from unity.

Another important feature of the rotational level structure in Fig. 3 is the termination of the series at each T, in contrast to a symmetric top where the series is infinite. This termination results from imposing the shell model restriction on the calculated levels. The shell model limits the number of $3l3l'3l''$ intrashell states. According to the shell model, for example, there is only one $3l3l'3l''$ intrashell state for $^2H^o$. Thus, even though there are two blank boxes ($T=1,5$) in Table II, only the $T=5$ component is occupied by this lowest state. Note that Table II was obtained without reference to the shell model. Clearly the number of rotational states increases if we consider higher intrashell triply excited states. For example, for $4l4l'4l''$ states the second $^2H^o$ state would occupy the $T=1$ blank box, and would appear as the next member of the $T=1$ series in Fig. 3, just above the $^2G^o(1)$ state. For the $2l2l'2l''$ triply excited states, group A has only four members, namely, the $L=1$ and $L=2$ states in Fig. 3 (see Ref. [11]). The symmetry also limits the allowed L's of

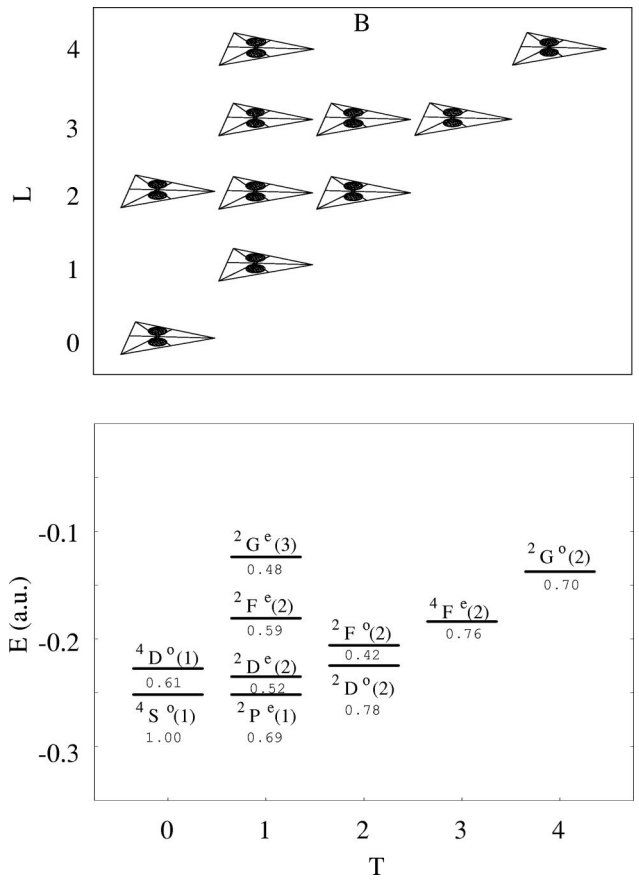

FIG. 4. Same as Fig. 3 but for group B elements.

the $T=0$ rotational series. For example, the $^4S^e$, $^4D^e$, and $^4G^e$ states are not allowed (see Table II).

In Fig. 3 we notice that there are two $^2G^e$ states; the first one was assigned to $T=4$, and the second one to $T=2$. The imaginary part of both T components has no nodal surfaces (see Table II). The lowest state favors higher T and the second state occupies the lower-T component, in accordance with the rotor energy formula [see Eq. (8) above].

The $^2G^o$ state in Fig. 3 also shows strong impurity. Since a small T implies higher rotational energy, this state acquires larger mixing from the higher $T=3$ and $T=4$ components, despite the fact that the nodal surfaces in these components would contribute to higher kinetic energy. In other words, the T component distribution is determined by the competition between the small T, which has higher rotational kinetic energy with no internal nodal surface, and the larger T, which has one internal nodal surface with higher internal kinetic energy.

C. Group B

After we have exhausted all the states that have nodeless rotational components, we turn to the next group, which has one nodal surface. We can distinguish the d type from the h and the s types, but the latter two cannot be distinguished from the density distribution $\rho_T(\Omega_I)$. From Table II, we select states whose components are labeled d and the corresponding value of T. The results are shown in Fig. 4. The fraction A_T is also indicated. These states form group B, but they were designated as group A_2' in Watanabe and Lin [6]. They are also identified by their highest corresponding T composition from Table II.

The resulting rotational level multiplet again resembles that of a symmetric top. As shown in Fig. 4, for each T, higher-L states have higher energies. However, for each fixed L, a state with larger T does not always have lower energy, as given by the rigid symmetric top expression of Eq. (8); see the $L=2$ and $L=3$ cases in Fig. 4. Unlike the states in group A, the rotational purity of states in this group is not high. For example, the $T=0$ component for the $^4D^o(1)$ state is 61% only. From Table I, the $T=1$ component for this state is 39%, with essentially no $T=2$ component. Such compositions can be understood from the nature of nodal surfaces summarized in Table II. For $^4D^o$, the $T=0$ component has a d node, the $T=1$ has an h or s node, while the $T=2$ has d +h or d+s nodes. Both $T=0$ and $T=1$ components have only one nodal surface such that both modes can be excited with comparable strength. The $T=2$ component has two nodal surfaces. It is less likely occupied by the lowest state. The same reasoning also explains the lack of good purity for the $^2P^e(1)$ state where $T=1$ is 69%, and $T=0$ is 31%. $T=1$ has a d node and $T=0$ has an h node; thus the mixing of these two components is not negligible. The lack of the well-behaved rotational level structure of a rigid symmetric top for group B is a reflection of the lack of good purity of the rotational components. The upper frame of Fig. 4, however, shows that $\rho_T(\Omega_I)$ for the indicated dominant T components do have identical shapes, i.e., they vanish at $\theta=\pi/2$, and thus the coplanar geometry is not allowed. The contour density distributions shown for this group resemble the distribution of an ammonia molecule NH_3. However this ''molecule'' is very ''floppy'' and deviation from the prototype ammonia molecule is not small due to the lightness of the electrons.

D. Group C

Next we identify states that are classified in group C (or group E' in Ref. [6]) where the dominant T component wave function has one s or h nodal surface, namely, one nodal surface at the equilateral triangle geometry. The internal excitation energies for states with such a nodal surface are likely to be about the same as for those states with a d nodal surface in group B.

In Fig. 5, states assigned to this group are shown, and the density distributions $\rho_T(\Omega_I)$ of the corresponding T are given in the upper frame. First we note that for $T\neq 0$ the rotational levels exist in pairs, one for quartet states and one for doublet states. The states in group C correspond to the degenerate vibrational modes for a molecule with D_{3h} symmetry, called the E' mode (see Ref. [6]).

The level diagram in Fig. 5 shows that the separation between rotational levels for a fixed T is less regular. Although for each fixed T higher-L states still have higher energies, the rotational energy level formula Eq. (8) for the rigid symmetric top is not followed. This is reflected by the fact that the rotational purity of some of these states is not

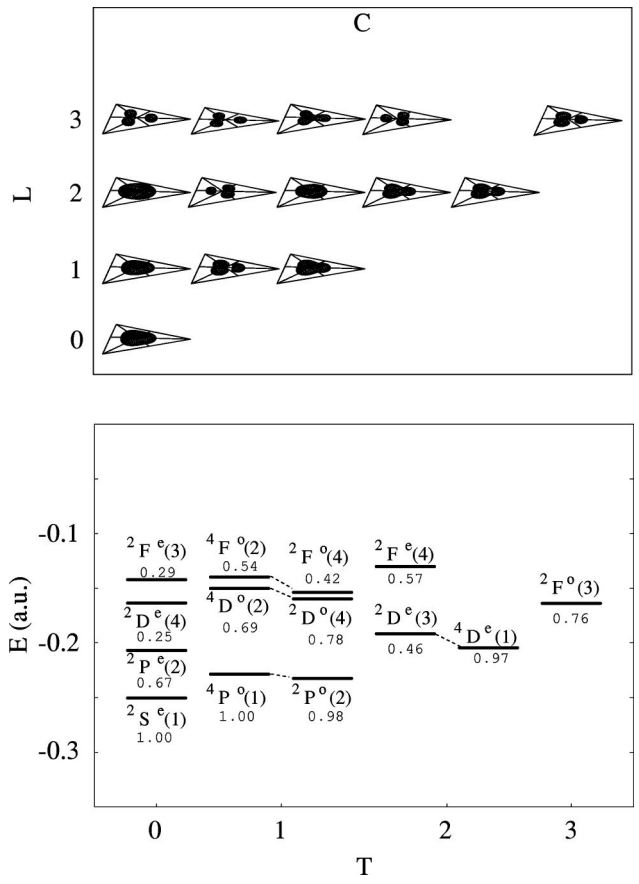

FIG. 5. Same as Fig. 3 but for group C elements.

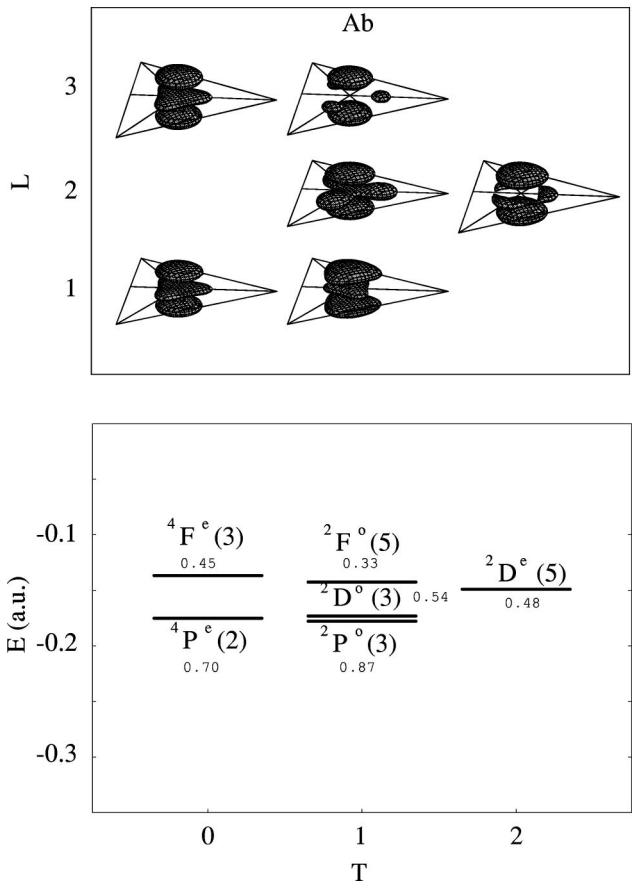

FIG. 6. Same as Fig. 3 but for group Ab elements. For the $^2D^e(5)$ state, the contour surface represents the equidensity surface of 20% of the maximum. For other states, the equidensity surface is 30% of the maximum. The $^{2S+1}L^{\pi}$ symmetry of the states of the rotational multiplet follows the pattern of Fig. 3 for group A.

good. Furthermore, the density plots for the assigned T components are not all identical as in Figs. 3 and 4. However, the dissimilarity is not very severe. Note that when the ''islands'' of the contour surfaces have significant overlap, it will appear as the torus seen in this figure. Recall that the density plots are surfaces of 60% of the maximum for each plot. When the density distribution is less sharply peaked, single contour surfaces may show larger differences. For this group, we consider the density plot shown for the $^4P^o(1)$ state as the prototype.

In constructing the rotational level structure in Fig. 5 we encountered some difficulties since the mixing of different T components is quite severe for some states. The assignment has been motivated more based on the symmetry analysis in Table II, with consideration of the rotational fractions A_T from Table I for the states assigned. The T assigned for some of the states does not have the largest rotational fraction. For example, both the third and fourth $^2D^e$ states have the largest $T=2$ component but the fourth state was assigned to $T=0$. This is based on the nature of nodal surfaces from Table II. For this symmetry, the lowest state is assigned to group A with $T=2$, which has no nodal surfaces. The second lowest state is assigned to group B with $T=1$ for its d nodal surface. The third state can occupy $T=0$ since it has an s nodal surface. However, the $T=2$ nodeless component can acquire one dynamical nodal surface which would have comparable excitation energy. In other words, all three T components have one nodal surface and all three T components are occupied, as shown by the comparable rotational fractions for the third and fourth states. When mixing is large, the assignment of a single T for the state is somewhat stretched.

E. Group Ab and group Ac

The classification so far includes states in group A where the major T component wave function has no nodal surfaces and states in group B and group C where the major T component has one nodal surface. We have assigned states in group B to have one d-type nodal surface at the coplanar geometry and states in group C to have one s- or h-type nodal surface at the equilateral triangle geometry.

We next consider states where the dominant rotational components have at least two nodal surfaces. Such states can be ''obtained'' by adding a d-type or an s- (h-)type nodal surface to the elements in group A. We name these groups Ab and Ac, respectively. In Figs. 6 and 7 we show the rotational levels and the density distributions $\rho_T(\Omega_I)$ for elements in group Ab (Ac). Note that the states in group Ab and in group Ac appear in parallel. In fact the L, S, and π states that form the rotational structure in groups Ab and Ac are built from the rotational levels of group A, except with the truncation determined by the shell model.

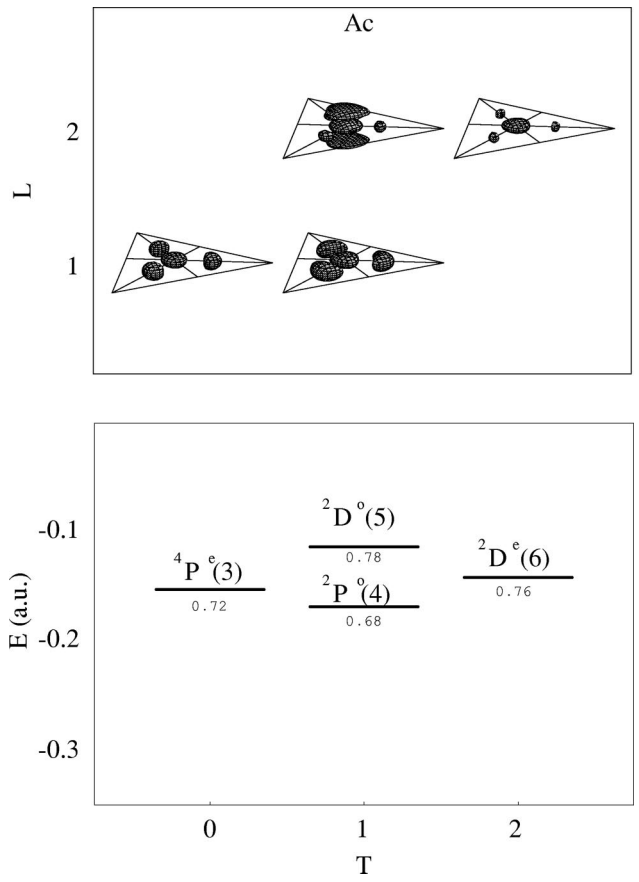

FIG. 7. Same as Fig. 6 but for group Ac. For the $^2D^o(5)$ state, the contour surface represents the equidensity surface of 20% of the maximum. For other states, the equidensity surface is 30% of the maximum.

The density distributions $\rho_T(\Omega_I)$ for the assigned T components for states in group Ab and group Ac are shown in the upper frames of Fig. 6 and Fig. 7, respectively. The variation of the densities within each group is much larger than those shown in groups A, B, and C, but the main features of the nodal surfaces do appear clearly.

For group Ab, we take the shape shown for the $^4P^e(2)$ state as the prototype. The coplanar surface is not a nodal plane as in group B, but rather an antinodal surface as in group A. However, d-type nodal surfaces occur twice, one above $\theta=\pi/2$ and the other below it. Thus for states in group Ab there are two nodal planes. Since an equilateral triangle appears to be the preferred shape, we plot the density distribution ρ_T as a function of θ at $\eta=2\pi/3$ and $\phi=0$ for the $^4P^e(2)$ state, as shown in Fig. 8(a). Clearly there are two nodes at θ about $\pi/12$ above or below $\theta=\pi/2$. In Fig. 6, apart from $^4P^e(2)$, $^2P^o(3)$, and $^4F^e(3)$ states, the density distributions for the other three states appear to differ from the prototype to a large extent. We attribute this to the mixing with other modes, as reflected by the small rotational fraction for the dominant T component in these states. From Fig. 6 we conclude that the rotational level structure of group Ab follows that of group A, but the dynamical nodal surfaces acquired belong to the types in group B. We use Ab to designate this group where the small letter b is used to imply

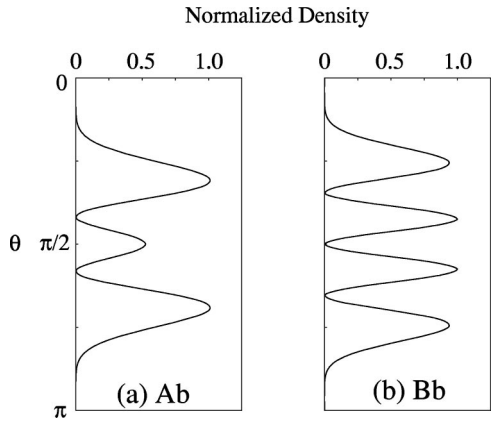

FIG. 8. The density distribution vs θ when the three electrons form an equilateral triangle ($\eta=2\pi/3$ and $\phi=0$). (a) For the $T=0$ component of the $^4P^e(2)$ state, showing that states in group Ab have two nodal planes. (b) Similar plot for the $T=0$ component of the $^4S^o(2)$ state, showing that states in group Bb have three nodal planes.

that the the dynamical nodal surfaces are of the type in group B.

The states assigned to group Ac are shown in Fig. 7. The prototype distribution of this group can be seen from the density plot of the $^4P^e(3)$ state. Comparing to the typical example in group C, say, the $^4P^o(1)$ state (see Fig. 5), the outer three ''islands'' in group Ac resemble the three islands in group C. On the other hand, in group Ac the density at the center (the coplanar equilateral triangle shape) is a local maximum, whereas in group C it is a node. For group Ac, separating the central maximum and each of the outer ''islands'' is a nodal surface. Note that the density distribution of the three ''islands'' in these plots implies a swing (or hinge) mode. While the three electrons can form a coplanar equilateral triangle, as they move away from this configuration, a dynamic nodal surface perpendicular to the η-ϕ plane similar to those for group C appears. The dynamic nodal surface can be seen more clearly by plotting the wave function on the η-ϕ plane at $\theta=\pi/2$, which will be addressed later in Sec. III G. Note that we use Ac to designate this group where the rotational level structure follows the pattern of group A, but the dynamical nodal surface belongs to the type in group C, so that the small letter c was used to designate this Ac group.

The density distributions for the states in group Ac shown in Fig. 7 are all very similar except for the $^2D^o(5)$ state. In fact, the latter has a shape closer to those in group Ab. However, an interchange of the two $^2D^o$ states between groups Ab and Ac is not desirable since the energy of the $^2D^o(5)$ state would become higher than the $^2F^o(5)$ state, upsetting the relative energy levels (higher L has higher energy for a fixed T) as expected from a ''rigid'' symmetric top. Since the deviation from a rigid symmetric top is large, neither assignment can be strictly ruled out.

F. Groups Bb, Cc, CB, Acc, and Ccc

The next groups consist of excited states built from group B or group C. In Fig. 9 we show group Bb, whose elements

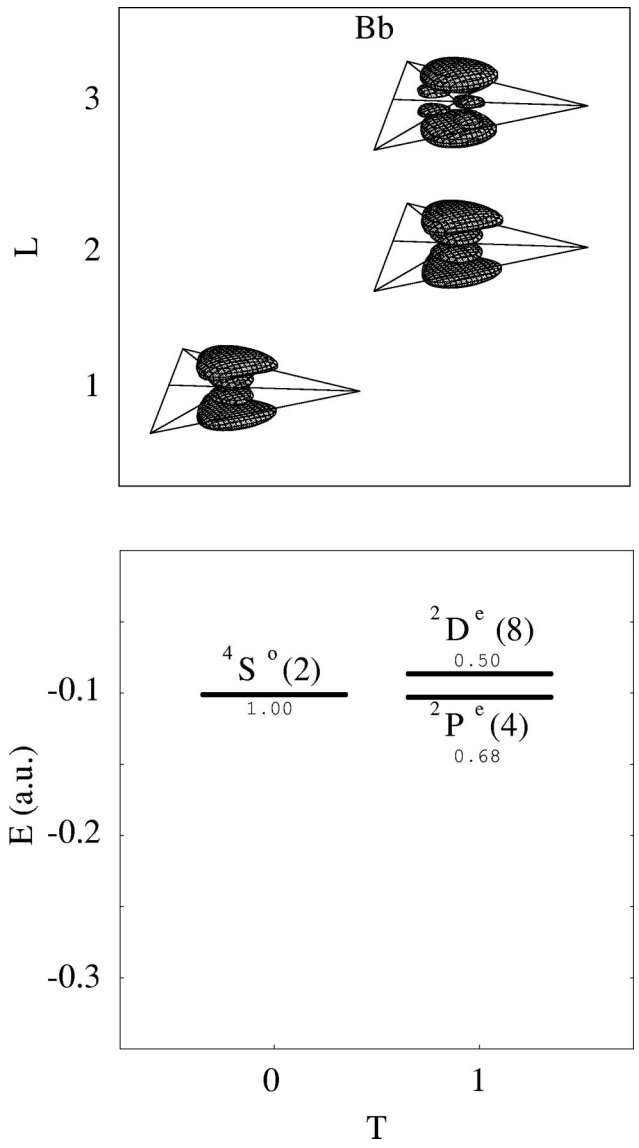

FIG. 9. Same as Fig. 3 but for group Bb. For the $^2D^e(8)$ state, the contour surface represents the equidensity surface of 20% of the maximum. For other states, the equidensity surface is 30% of each maximum.

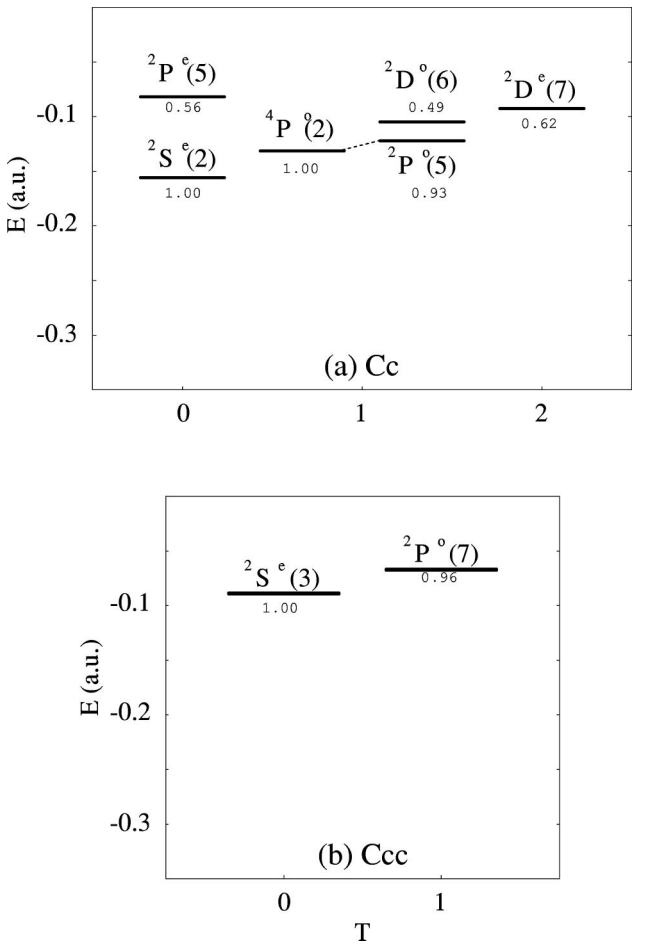

FIG. 10. (a) The rotational level pattern of states in group Cc. (b) The rotational level pattern of states in group Ccc. The number of states is limited due to the shell model restriction for the $3l3l'3l''$ states.

are built from group B. The designation B explains that states in this group have a nodal surface at $\theta=\pi/2$, as in those states in group B. The rotational level structure should follow that of group B as well. The second b designation implies that the dynamic nodal surface is of the group B type, adding one extra nodal surface above and one below the $\theta=\pi/2$ plane. These nodal surfaces can be seen in the upper frame of Fig. 9. From the figure, it appears that the equilateral triangle is the preferred shape at any θ. Thus we plot the θ dependence of the density distribution ρ_T at $\eta=2\pi/3$ and $\phi=0$ for the prototype state $^4S^o(2)$ in Fig. 8(b). The three nodes are clearly seen, one at $\theta=\pi/2$, and the other two at about $\pi/6$ above and below it.

Similarly we can build group Cc based on group C by adding an extra dynamic c nodal surface to the dominant rotational components for elements in group C. The rotational level pattern will follow that of group C and we have identified six elements of this group in Fig. 10(a). Since the densities for these excited states are not well localized the contour surface plots do not reveal the major features. We will defer the discussion of nodal structures for this group to the next subsection.

We also have group CB and the four elements in this group are shown in Fig. 11. These elements have nodal surfaces of the types d+s and/or d+h in Table II. Since the nodal surfaces are mainly due to the inherent quantum symmetry, rather than from the dynamic one, we use CB to designate this group. Note that the rotational level structure of this group shows the doublet pattern of the elements in group C for $T\neq 0$; thus they are designated as group CB according to our convention. Compared to the density distribution for elements in group C, in this group the distribution is obtained by adding an extra nodal plane at $\theta=\pi/2$.

We have also identified elements that are classified in group Acc and and in group Ccc. These are highly excited states within the manifold and their numbers are severely limited by the truncation imposed by the shell model. For the Ccc group we identified two elements as shown in Fig.

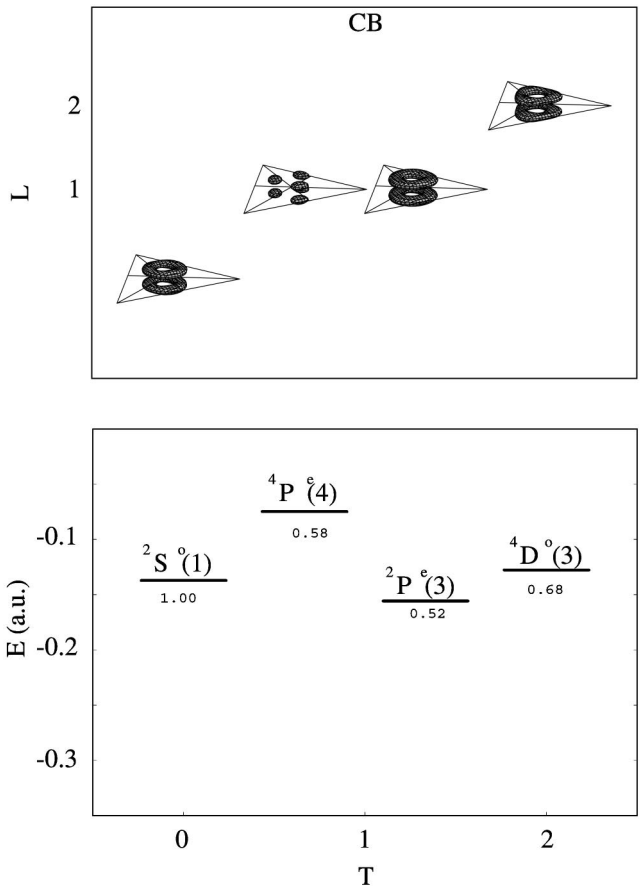

FIG. 11. Similar to Fig. 3 but for elements in group CB.

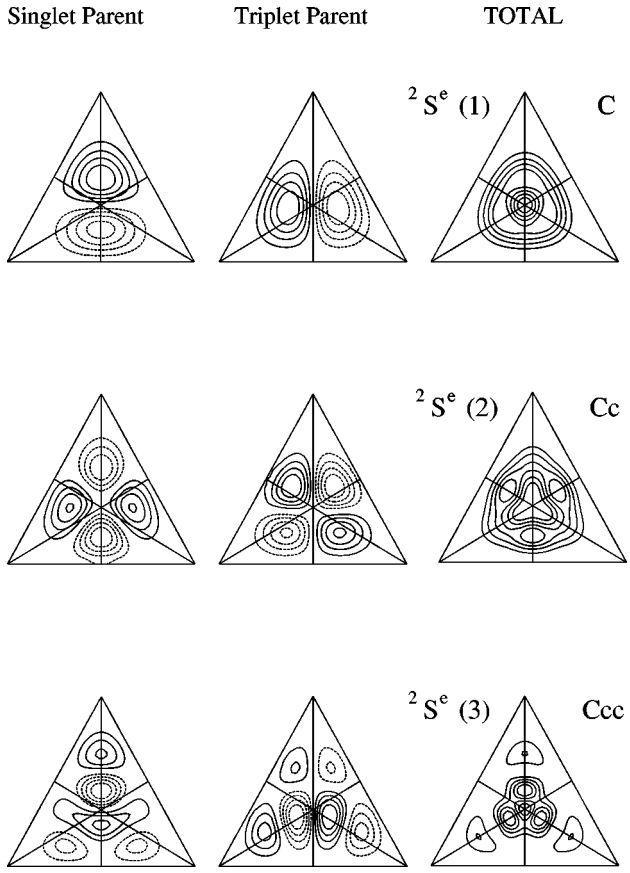

FIG. 12. Gray-scale contour plots of the wave functions of the three $^2S^e$ states on the $\theta=\pi/2$ plane. Both the singlet parent and triplet parent component wave functions are shown. Only the real part of the wave function is displayed since the imaginary part vanishes identically. The three states belong to groups C, Cc, and Ccc, respectively, and the number of nodal lines increases as the excitation energy is increased. The total density is shown to the far right.

10(b). For the Acc group, we identified only one element, $^2P^o(6)$, which has $T=1$. Note again that the rotational level structure for elements in Ccc follows the pattern for group C, and for elements in Acc follows the pattern for group A, despite the fact that the number of states is quite limited in each case.

G. Nodal surfaces for states in groups C, Cc, Ccc, and groups A, Ac, Acc at the coplanar geometry

We have attempted to display the contour surfaces of the density distributions for elements in groups Cc, Acc, and Ccc. As stated earlier, the distributions for these states are not very localized and contour plots do not reveal the major features. For the elements in groups C, Cc, Ccc, Ac, and Acc, the major distinctions can be seen from the wave functions on the equatorial plane, $\theta=\pi/2$. Since the three $^2S^e$ states are classified in groups C, Cc, and Ccc, respectively, we examine the wave functions of these three states. From Table II, the imaginary part of the wave function for $^2S^e$ is identically zero; thus we need to show the real part of the wave function only. We show both the singlet parent and the triplet parent components, even though the triplet parent component can be obtained directly from the singlet parent component via symmetry transformation by the projection operators of the S_3 group. In any event, in Fig. 12 we show the contour plots of the singlet and triplet parent component wave functions $\varphi_{LQ}^{S,S_{12}}(\Omega_I)$ and the total density distributions $\rho_T(\Omega_I)$ for the three $^2S^e$ states on the equatorial plane. Solid vs dotted contour lines are used to distinguish positive and negative values of the wave functions. Consider the triplet parent component only. For the lowest state in group C, $\phi=0$ [the vertical diagonal line in the figure; see Fig. 2(c)] is a nodal line, meaning that it does show the motion of a swing mode. For the second state, which is in group Cc, there is an additional nodal line perpendicular to the $\phi=0$ plane at $\eta=2\pi/3$. This is a hinge mode. For the third state, which belongs to group Ccc, we can identify three nodal lines (the three nodal lines are more clearly seen in the singlet parent component wave function). From the figures, we note that, although each singlet parent or triplet parent component wave function has well-defined nodal structure, the nodal surfaces are not as pronounced in the total density plots.

We next consider the wave functions for the $^2P^o$ states on the equatorial plane. The nodal surfaces for the first and the third states, being in group A and group Ab, respectively, are

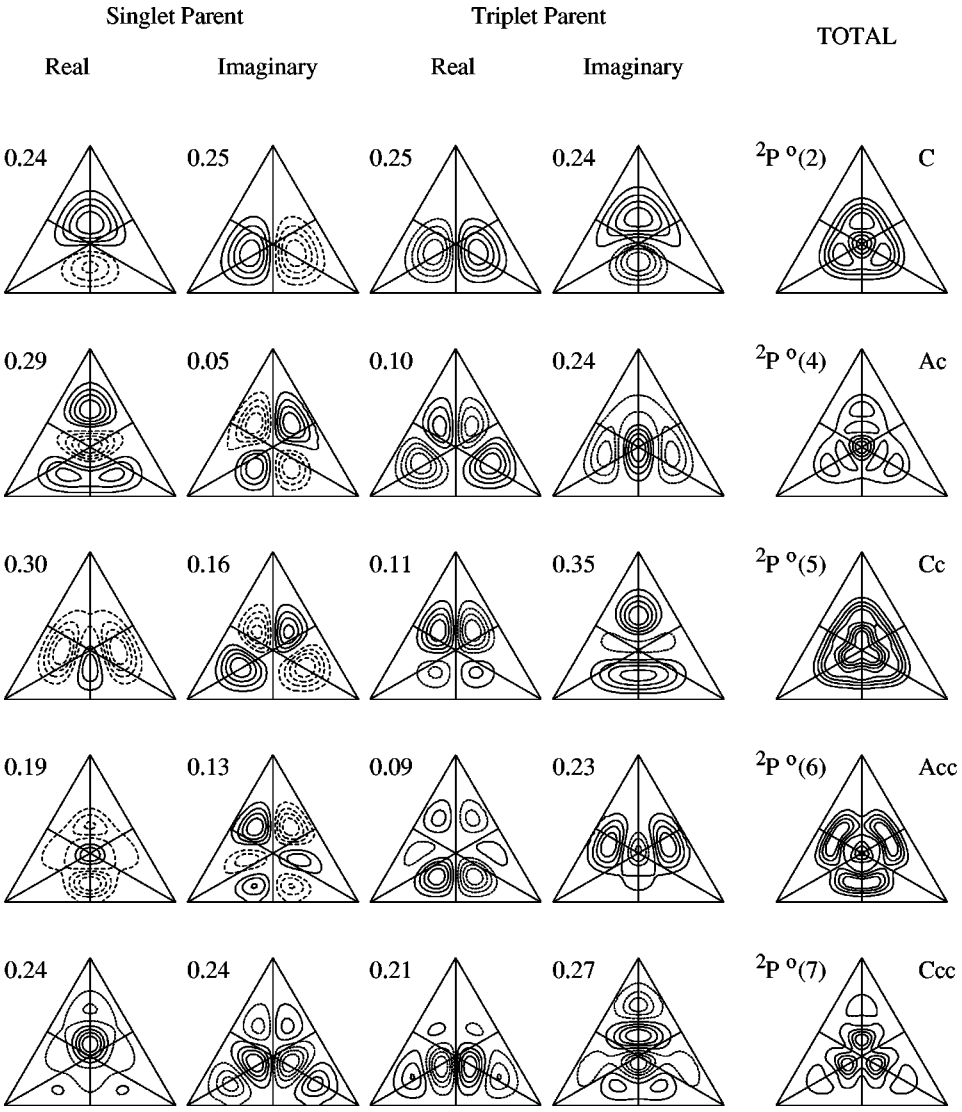

FIG. 13. Gray-scale contour plots for the $T=1$ component wave functions for the second, fourth, fifth, sixth, and seventh $^2P^o$ states. The real and the imaginary parts of the wave functions for both the singlet and triplet parents are plotted and the fractional contributions of each component to the $T=1$ total density are shown. These states belong to groups C, Ac, Cc, Acc, and Ccc, respectively. Note the increasing number of nodal lines as the excitation energy is increased. The plot is for $\theta=\pi/2$.

quite easy to understand. The remaining five states are best investigated by examining the nodal structure of the wave functions on the η-ϕ plane at $\theta=\pi/2$. From Table I, we have assigned the second, fourth, fifth, sixth, and seventh states to groups C, Ac, Cc, Acc, and Ccc, respectively, with $T=1$. In Fig. 13, we show the real part and the imaginary part of the singlet parent and triplet parent component wave functions $\varphi_{LQ}^{S,S_{12}}(\Omega_I)$ for each state and the total density $\rho_T(\Omega_I)$ is shown at the far right. The singlet parent components can be obtained through an S_3 transformation from the triplet parent components in principle. Thus we will focus only on the triplet parent components. In Fig. 13 we show the rotational fractions decomposed into the real part and the imaginary part as well. For the second state, which is in group C, both the real and imaginary parts have one nodal line. For the fourth state, which is in group Ac, the real part has two nodal lines and the imaginary part has one nodal line, with 10% and 24% fractions, respectively. For the fifth state, which belongs to group Cc, both the real and the imaginary parts have two nodal lines. For the sixth state, which is a member of group Acc, the real part has three nodal lines and the imaginary part has two nodal lines. For the seventh state, which is a member of group Ccc, both the real part and the imaginary part have three nodal lines. Thus the energy ordering of the second, fourth, fifth, sixth, and seventh states can be understood in terms of the increasing nodal lines on the η-ϕ plane in the $T=1$ component. The third state is different in that it is characterized by two nodal planes in the angle θ. Since the wave functions for these excited states are more diffuse, the total density distributions do not show pronounced localized structure and contour surfaces are not illustrative in displaying the internal structure of the states. On the other hand, the relative energy ordering of the model atom can be understood in terms of the increasing number of nodal surfaces in the internal wave functions.

As an additional comment, we compare the wave functions of the $^2S^e$ states in Fig. 12 with the $^2P^o$ states that belong to the C, Cc, and Ccc groups in Fig. 13. Note that the real parts of the singlet parent and the triplet parent component wave functions for the $^2S^e$ states are very similar to the corresponding $T=1$ components for the paired $^2P^o$ states. This forms the basis of the present assignment.

IV. THE CLASSIFICATION OF INTRASHELL TRIPLY EXCITED STATES OF ATOMS

A. The classification of the $3l3l'3l''$ states of the model atom

Based on the analysis of nodal surfaces of the wave functions we have tentatively classified all the 64 states of the model atom and the results are summarized in Table I. The present classifications are listed in the second column of this table where each state is denoted by a group such as A, B, Ab, Acc, etc., and a quantum number T. It is understood that some features of the classification may be violated in real atoms. However, it is the regularity that we are looking for and we would like to see to what extent the intrashell $3l3l'3l''$ triply excited states of atoms can be classified using this scheme.

Before making the comparison, it is appropriate to comment on the connection between the present model atom and the intrashell states of a real atom. As shown from our previous results on the $2l2l'2l''$ intrashell states of Li using hyperspherical coordinates [11,12], the wave functions of the real atom at $r_1=r_2=r_3$ are essentially identical to those from the model atom employed here. In a real atom, the radial distances of the three electrons do not have to stay equal, but each radial distance deviates only slightly from the optimum value r_0 used here. Meanwhile, the wave function should reach near a maximum at $r_1=r_2=r_3$ for intrashell states. Since each wave function is not expected to change rapidly as the radial distances are varied, the conclusion based on the present model atom should be a good approximation for the intrashell triply excited states. We comment that a similar model atom was used successfully earlier to study the properties of intrashell doubly excited states of a two-electron atom [31].

B. The classification of triply excited states of N^{4+}, N^{2+} and He^-

A true test of the validity of the present classification based on the model atom is to check if the energy levels of the $3l3l'3l''$ triply excited states of atoms and ions indeed can be classified by the present scheme. There are very few experimental data for $3l3l'3l''$ triply excited states for any atoms or ions. Likewise, theoretical data obtained by different methods are also very limited. The most recent extensive calculations where each eigenstate is separately computed and optimized are the 11 states reported by Nicolaides and Piangos [25] for He^-. In this calculation, however, they obtained only states with parity $\pi=(-1)^L$. No calculations have been reported for states with $\pi=-(-1)^L$. Fortunately, there is at least one calculation where all the 64 $3l3l'3l''$ triply excited states have been reported. The data are from Vaeck and Hansen [26] for N^{4+} based on the configuration-interaction approach. It is difficult to assess the accuracy of such calculations since only limited configurations can be included in the calculation. However, their data offer us an opportunity to check how well the present classification scheme can be applied to the N^{4+} ion. In their paper, Vaeck and Hansen attempted to classify the states they calculated using the limited classification scheme of Watanabe and Lin [6], where many states at higher energies were left as ''residues.'' In the present classification, every state has been assigned (or classified).

With the present scheme, the assignment of each calculated state is straightforward. Following Table I and the order of the energy levels of each state, the group in which the state belongs and the T assigned are read off from the table. The calculated energy levels are then arranged for each group A, B, C, Ab, . . . , separately. The energy level of each state within the group is then ordered according to the T assigned to obtain the rotational structure.

We applied such assignment to the the $3l3l'3l''$ triply excited states of N^{4+} calculated from Vaeck and Hansen [26] and ordered their energies according to the different groups and T. The results are shown in Fig. 14. In Fig. 14(a) we show the rotational structure of states belonging to groups A, Ab, Ac, and Acc. One can see that within each group the relative energy levels are similar to those shown for the model atom with minor differences. Within each group and fixed T, the state with higher L has higher energy. The relative energies for states with fixed L but different T, however, do not follow the levels of a rigid symmetric top. We emphasize once again that the states in groups Ab, Ac, and Acc follow the order of the states in group A, except for the truncation at the higher states. This truncation is determined by the shell model. Similarly, we also show groups B and Bb in Fig. 14(b) where the states in the two groups follow the same pattern as for the model atom. We also list the states from group CB here for a concise presentation. This is a separate group and has different level structures. We show groups C, Cc, and Ccc in Fig. 14(c). Note the near degeneracy of pairs of states with identical L for $T\neq 0$. They are from the doubly degenerate representation of the symmetry group E' of group D_{3h} (see Watanabe and Lin [6]).

A careful examination of the levels in Fig. 14 reveals two ''irregularities'' in the relative energies along a fixed T. The first is the inversion of the order between $^2D^o(3)$ and $^2P^o(3)$ in group Ab ($T=1$). The other is between $^4F^o(2)$ and $^4D^o(2)$ in group C ($T=1$). According to the CI coefficients calculated by Vaeck and Hansen [26] the dominant configuration for the $^2D^o(3)$ state is $3s3p(^1P^o)3d$ and for $^2P^o(3)$ is $3s3p(^3P^o)3d$. If the single configuration of $3s3p3d$ is a correct representation for these two states, then the energy of the $^2D^o(3)$ state should be lower than the $^2P^o(3)$ state in accordance with Hund's rule, which says that larger L has lower energy if the spin is the same. Thus the calculated energies for these two states are consistent with the shell model, even though configuration mixing has been found to be quite large for both states. In the other pair, Vaeck and Hansen showed that the $^4D^o(2)$ state has 88% of the $3d^2(^3P^e)3p$ configuration and the $^4F^o(2)$ has 96% of the $3d^2(^3F^e)3p$ configuration. In this case configuration mixing is small and the relative energy order from the calculation is consist with Hund's rule for the $3d^23p$ configuration. It should be pointed out, however, that the validity of Hund's rule for configurations with more than one open shell is quite limited and cannot be expected on general grounds.

Vaeck and Hansen have also obtained the energy levels of $1s^23l3l'3l''$ triply excited states of N^{2+}. We classify these

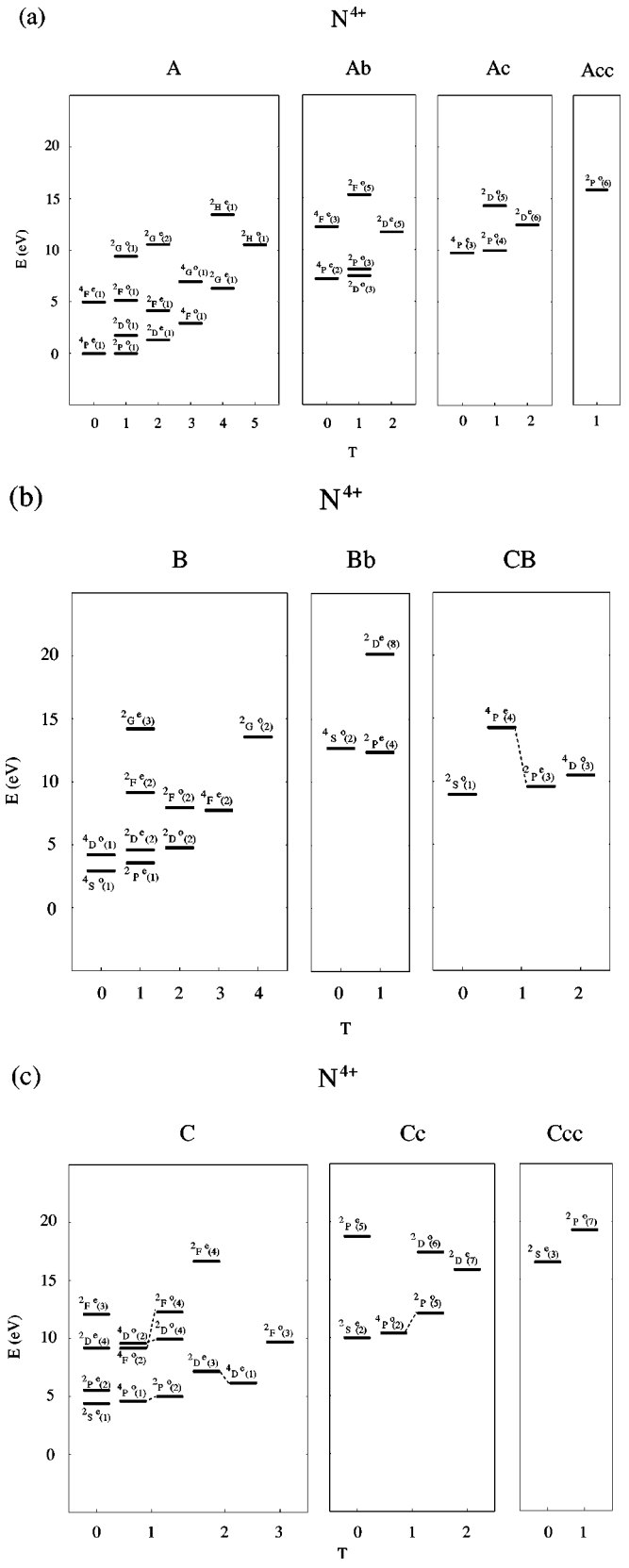

FIG. 14. Energy levels of intrashell $3l3l'3l''$ triply excited states of N^{4+} regrouped according to the present classification scheme. Each group shows the rotational level structure similar to that of the model atom. The energy levels are taken from the calculations of Vaeck and Hansen [26].

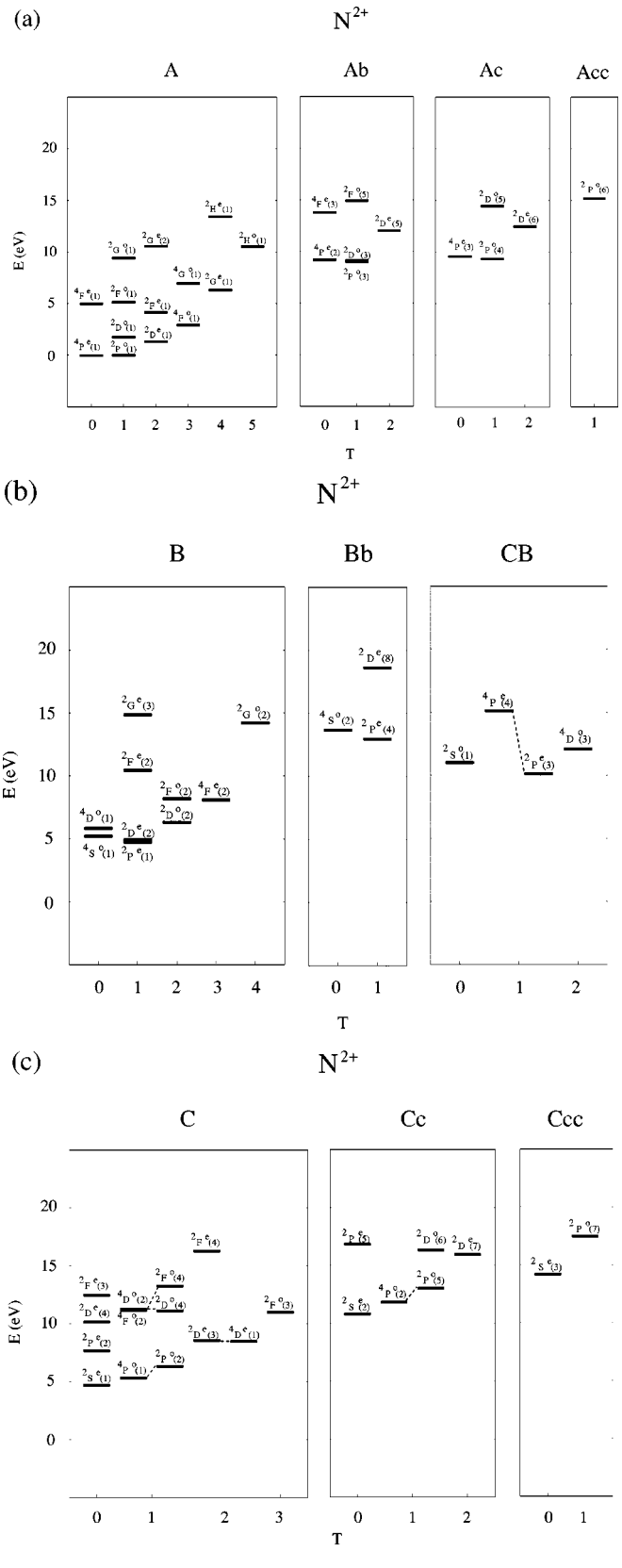

FIG. 15. Similar to Fig. 14 except for the $1s^23l3l'3l''$ triply excited states of N^{2+}.

states also using the scheme for the model atom. The results are shown in Fig. 15. Note that the relative energy order along each fixed T follows the pattern of the model atom. In this case we did not find any ''irregularities.'' We have also checked the 11 states calculated by Piangos and Nicolaides [25] for He^-. The number of states obtained is too small, but their relative pattern is identical to that of the model atom. In fact, this is not surprising since the model atom is obtained for the limit where interelectronic interaction is of paramount importance. Deviations from the present scheme are expected to be more frequent as the nuclear charge Z increases. However, as shown in Fig. 14, the number of ''violations'' is still very few for N^{4+}. This shows that the present classification has a wide region of validity.

It should be pointed out that the present classification scheme is not limited to the $3l3l'3l''$ states. In fact, the present scheme includes the classification of the $2l2l'2l''$ states, as shown in our earlier work where the eight states can be separated into four states in group A, two states in group B, and two states in group C. The groups identified so far will appear in the $4l4l'4l''$ triply excited states; each group will include more states with higher L. There will be additional groups, corresponding to states with higher dynamical excitations. These groups can be extracted in a procedure similar to the one used here.

V. SUMMARY AND DISCUSSION

In this paper we obtained the accurate wave functions of a model three-electron atom with each electron confined to the surface of a sphere with radius r_0. The eigenstates of such a model atom were calculated and were used to approximate the $3l3l'3l''$ triply excited states of He^- when r_0 was set equal to 6.326 a.u. The wave functions of the states that would approximate the 64 intrashell $3l3l'3l''$ triply excited states of a real atom were then examined in the body-fixed frame and the rotation-averaged (with respect to the laboratory-fixed axes) density distributions were analyzed. With the aid of symmetry analysis, we assigned all the 64 states into different groups. Each group is approximately characterized as analogous to the specific bending vibration of an XY_3 molecule. Three basic normal modes have been identified and the excitations of these basic modes have been enumerated for the 64 states calculated. They have been classified into A, B, C, Ab, Ac, Bb, CB, Cc, Acc, and Ccc groups, where the capital letters are used to denote the basic normal modes and the small letters are used to denote dynamic excitations in that mode. Each intrashell triply excited state is classified to belong to one of the groups, together with the projection of its total orbital angular momentum in the direction perpendicular to the plane of the three electrons. These classifications for the 64 intrashell $3l3l'3l''$ triply excited states are listed in Table I. These classifications are to replace the designation based on the independent electron model where strong configuration mixing renders the shell model designation meaningless. The classification scheme is then shown to classify well the intrashell $3l3l'3l''$ states of N^{4+} and the $1s^23l3l'3l''$ states of N^{2+}. The present method, similar to what has been achieved for doubly excited states of atoms [1], derived the classification scheme by examining the internal wave functions, or, equivalently, the correlation properties of the electrons. With this classification scheme, the seemingly irregular spectra can be regrouped in order. While the classification scheme appears to be complete for the $3l3l'3l''$ triply excited states from the present work, additional possible systematic behaviors in the autoionization widths or radiative rates are waiting to be discovered in the future.

ACKNOWLEDGMENTS

T.M. wishes to thank Professor M. Matsuzawa and Professor S. Watanabe for their encouragement throughout this work. This work was supported in part by Chemical Sciences, Geosciences and Biosciences Division, Office of Basic Energy Sciences, Office of Science, U.S. Department of Energy and also in part by a Grant-in-Aid for Scientific Research, Ministry of Education, Science, and Culture, Japan.

[1] C. D. Lin, in *Review of Fundamental Processes and Applications of Atoms and Ions*, edited by C. D. Lin (World Scientific, Singapore, 1993).
[2] C. D. Lin, Phys. Rev. A **29**, 1019 (1984).
[3] D. R. Herrick, Adv. Chem. Phys. **52**, 1 (1983).
[4] J. M. Rost and J. Briggs, J. Phys. B **24**, 4293 (1991).
[5] J. E. Hunter and R. S. Berry, Phys. Rev. A **36**, 3042 (1987).
[6] S. Watanabe and C. D. Lin, Phys. Rev. A **36**, 511 (1987).
[7] C. G. Bao, X. Z. Yang, and C. D. Lin, Phys. Rev. A **55**, 4168 (1997).
[8] C. A. Nicolaides, N. A. Piangos, and Y. Komninos, Phys. Rev. A **48**, 3578 (1993).
[9] T. Morishita and C. D. Lin, Phys. Rev. A **57**, 4268 (1998).
[10] T. Morishita and C. D. Lin, J. Phys. B **31**, L209 (1998).
[11] T. Morishita, Y. Li, and C. D. Lin, Phys. Rev. A **58**, 4214 (1998).
[12] T. Morishita and C. D. Lin, Phys. Rev. A **59**, 1835 (1999).
[13] L. M. Kiernan *et al.*, Phys. Rev. Lett. **72**, 2359 (1994); J. Phys. B **28**, L161 (1995).
[14] L. Journal *et al.*, Phys. Rev. Lett. **76**, 30 (1996).
[15] Y. Azuma *et al.*, Phys. Rev. Lett. **74**, 3768 (1995).
[16] S. Diehl *et al.*, Phys. Rev. Lett. **84**, 1677 (2000).
[17] K. Berrington and S. Nakazaki, J. Phys. B **31**, 313 (1998).
[18] H. L. Zhou, S. T. Manson, P. Faucher, and L. Vo Ky, Phys. Rev. A **62**, 012707 (2000).
[19] Y. Zhang and K. T. Chung, Phys. Rev. A Phys. Rev. A **58**, 3336 (1998), and references therein.
[20] G. Verbockhaven and J. E. Hansen, Phys. Rev. Lett. **84**, 2810 (2000).
[21] C. A. Nicolaides, N. A. Piangos, and Y. Komninos, Phys. Rev. A **48**, 3578 (1993).
[22] Y. Azuma *et al.*, Phys. Rev. Lett. **79**, 2419 (1997).
[23] S. Diehl *et al.*, Phys. Rev. A **56**, R1071 (1997).
[24] H. Bachau, J. Phys. B **29**, 4365 (1996).

[25] C. A. Nicolaides and N. A. Piangos, J. Phys. B **34**, 99 (2001).
[26] N. Vaeck and J. Hansen, J. Phys. B **25**, 883 (1992).
[27] C. G. Bao, J. Phys. B **25**, 3725 (1992).
[28] C. G. Bao and C. D. Lin, Phys. Rev. A **52**, 3586 (1995).
[29] C. G. Bao, Few-Body Syst. **13**, 41 (1992).
[30] T. Morishita and C. D. Lin, J. Phys. B **34**, L105 (2001).
[31] G. S. Ezra and R. S. Berry, Phys. Rev. A **28**, 1974 (1983).